

Rapeseed population point cloud completion network (RP-PCN) with dynamic graph convolution for 3D reconstruction of crop canopy occlusion architecture

Ziyue Guo^{a,b}, Xin Yang^{a,b}, Yutao Shen^{a,b}, Yang Zhu^c, Lixi Jiang^c, Haiyan Cen^{a,b,*}

^a *College of Biosystems Engineering and Food Science, Zhejiang University, Hangzhou 310058, P.R. China*

^b *Key Laboratory of Spectroscopy Sensing, Ministry of Agriculture and Rural Affairs, Hangzhou 310058, P.R. China*

^c *College of Agriculture and Biotechnology, Zhejiang University, Hangzhou 310058, P.R. China*

* *Correspondence: hycen@zju.edu.cn; Tel: +86-571-8898-2527*

Abstract

Quantitative descriptions of the complete canopy architecture are essential for accurately evaluating crop photosynthesis and yield performance to guide ideotype design. Although various three-dimensional (3D) sensing and modeling technologies have been developed for 3D reconstruction and characterization of individual plants and canopies, they failed to obtain a complete and accurate description of canopy architecture due to severe occlusion among crop organs and complex canopy architectures. In this study, we proposed a novel point cloud complete model for accurate 3D reconstruction of plot-level rapeseed population from seeding to silique stages with multi-view imaging. We first developed a complete point cloud generation framework to obtain a high-quality training dataset via the virtual-real integration (VRI) simulation method combined with the occlusion point detection algorithm, enabling

automated annotation of the training dataset by distinguishing surface points from occluded points within canopies. The rapeseed population point cloud completion network (RP-PCN) was then designed with a multi-resolution dynamic graph convolutional encoder (MRDG) and a point pyramid decoder (PPD) to predict occluded points based on the input surface point clouds. To further enhance feature extraction, a dynamic graph convolutional feature extractor (DGCFE) module was proposed to capture structural variations over the whole rapeseed growth period. The effectiveness of point cloud completion was validated by predicting yield using architectural indicators from complete point clouds of rapeseed population. The results demonstrated that RP-PCN achieved chamfer distance (CD) values of 3.35 cm, 3.46 cm, 4.32 cm, and 4.51 cm at the seedling, bolting, flowering, and silique stages, respectively, outperforming the state-of-the-art Transformer-based method (PoinTr) across all growth stages. Ablation studies confirmed the effectiveness of the MRDG and DGCFE modules, reducing CD values by 10% and 23%, respectively. Moreover, the silique efficiency index developed from RP-PCN improved the overall accuracy of rapeseed yield prediction by 11.2% compared to that of using incomplete point clouds. The RP-PCN pipeline proposed in this study has the potential to be extended to other crops, significantly enhancing the analysis of population canopy architectures and advancing high-throughput plant phenotyping in field environments.

Keywords

Plant phenotyping; 3D reconstruction; population simulation; point cloud completion; yield estimation

1. Introduction

Breeding rapeseed (*Brassica napus* L.) cultivars that are adapted to dense planting and high-yielding is an essential goal in developing cash crops that do not compete with staple food crops for land (Zheng et al., 2022). Crop canopy architecture plays a crucial role in achieving these traits, as the number, size, and spatial arrangement of canopy leaves directly influence light distribution and interception, thereby affecting photosynthetic efficiency and ultimately impacting yield (Liu et al., 2021). In sparse canopies, horizontal leaves maximize light interception, whereas in dense canopies, an ideotype plant display upright leaves at the top and progressively horizontal leaves in deeper layers, optimizing light utilization efficiency. Additionally, canopy architecture influences the microenvironment within the crop population. Overly dense canopies restrict air circulation, increasing the risk of disease, while sparse canopies fail to meet high-yield requirements (N. Li et al., 2022). However, quantitative descriptions of canopy architecture that contributes to conducting ideotype design to improve photosynthesis and yield, especially for rapeseed crops with large canopy architecture diversity across the entire growth period, remains a great challenge.

Recently development of high-throughput plant phenotyping with three-dimensional (3D) imaging and reconstruction methods provides an opportunity to characterize crop canopy architecture. These techniques include depth camera, laser scanning, LiDAR, and multi-view imaging. Reported studies have used the depth camera in plant phenotyping systems for 3D data acquisition, enabling the extraction of key structural parameters such as the leaf count and the leaf area of tomato plants

(Masuda, 2021; Watawana and Isaksson, 2024). Hand-held laser scanner was also utilized to capture fine-scale 3D point clouds of individual rapeseed plants at the maturity stage, allowing the extraction of structural information such as silique volume and length (Ma et al, 2023). While these methods are limited by the imaging conditions required by the sensors and their detection range, making them suitable only for reconstructing simple targets such as individual plants or greenhouse crops. Active LiDAR systems combined with unmanned aerial vehicle (UAV) provide an alternative for acquiring large-scale crop canopy point clouds at the plot or field scale, achieving accurate extraction of maize crop structural parameters such as plant height with the coefficient of determination ($R^2 > 0.97$) and leaf area index of $R^2 = 0.96$ (Bailey and Mahaffee, 2017; Jin et al., 2021). While the high cost and light absorption issues of LiDAR at the emission wavelength limits its applications to obtain detailed features of canopy internal architecture. Thanks to the fast development of deep learning, and multi-view imaging combined with recent emergence of advanced deep learning algorithms such as neural radiance fields (NeRF), has significantly improved the accuracy of 3D crop reconstruction from multi-view images, facilitating successful 3D reconstruction of crops in both greenhouses and field environments (Arshad et al., 2024). With the additional color information and easy to fuse with other sensing data, multi-view imaging-based 3D reconstruction has been widely utilized in the extraction of various canopy structural parameters (M. Li et al., 2022; Rossi et al., 2022). However, due to severe occlusion within the canopy, particularly in the late growth stages, it is still unable to capture the complete canopy architecture, especially the internal parts.

To address these challenges, an ideal approach is to quantitatively describe the spatial architecture of plants and then use computer graphics techniques to generate virtual crop models with complete canopy architectures. Murchie and Burgess (2022) analyzed the photosynthetic efficiency of crops under different virtual canopy architectures by modifying leaf distribution, providing a theoretical basis for ideotype plant design. While crop growth is influenced by various environmental factors, making it difficult to precisely quantify the variations in canopy architecture, leading to simulated results that often fail to accurately reflect real-world conditions. Reported studies have attempted to use shape-fitting methods to complete occlusive parts at the plant organ-level. Ge et al. (2020) achieved point cloud completion for occlusive fruits using predefined topological rules. The completed strawberry point cloud demonstrated a high intersection over union (IoU) of 0.77 compared to the ground truth. Lou et al. (2022) used biological constraints to complete occlusive leaf point cloud. Based on the completed lettuce point clouds, the R^2 value of the projected leaf area increased from 0.741 to 0.911, while the R^2 for total leaf area estimation improved from 0.338 to 0.964. These methods rely on limited prior knowledge and quantitative descriptions of structured objects, making them suitable only for organs with symmetrical architectures.

With the development of deep learning, significant advancements have been made in point cloud completion tasks, primarily driven by large datasets and improvements in network design. Many studies have made their 3D datasets publicly available, from which random clipping can be applied to generate a large number of training samples, providing a solid foundation for point cloud completion models (Geiger et al., 2013;

Tchapmi et al., 2019; Wu et al., 2015). To address the unordered and unstructured nature of point clouds, some studies have designed various networks for feature extraction, including point-based multi-layer perceptron (MLP), graph-based structures, transformer-based models, and voxel-based convolutions (Fei et al., 2022; Huang et al., 2020; Xie et al., 2020; Yu et al., 2021). These methods have achieved good completion results on public datasets, most of which consist of rigid objects such as vehicles and furniture. In the agricultural domain, point cloud completion studies have primarily focused on simpler structures, such as fruit or potted plant organs. Magistri et al. (2024a) designed a transformer-based model combined with template matching to complete point clouds of occlusive sweet peppers and strawberries obtained from single-view depth images. Similarly, Chen et al. (2023) successfully applied the point-based PF-Net model to complete leaf point clouds, obtaining complete leaf structures from top-down depth camera images of potted cabbage. Likewise, Zhang et al. (2023) incorporated the MSGRNet+OA module into the convolution-based GRNet to successfully complete the occlusive parts of corn leaves scanned by LiDAR. Existing point cloud completion models are typically designed to extract structural features at fixed scales, which limits their ability to dynamically adapt to the evolving plant architecture across different growth stages, particularly for complex crop canopies with overlapping leaves and spatial heterogeneity.

In summary, the current approaches still remain a great challenge to obtain an accurate rapeseed population complete point cloud throughout the entire growth period. First, there is a lack of large, comprehensive plant population point cloud datasets with

complete canopy architectures, which are essential for training robust models. Second, current dataset generation methods fail to represent the true nature of occlusive internal points in rapeseed canopy point cloud, which are the main target for completion, rather than randomly missing surface points. Finally, the architecture of point cloud completion networks that can effectively handle complex plant canopy architectures, particularly those involving dense and irregular geometries, remains an open question. To address these challenges, this study makes the following contributions:

(i) We generated a simulated rapeseed population dataset with complete canopy architectures by combining 3D data collected from individual rapeseed plants grown in field conditions with a breeding plot planting pattern. Additionally, we developed an occlusion point detection algorithm to create a point cloud completion dataset that closely reflects real-world conditions.

(ii) We designed a rapeseed population point cloud completion network (RP-PCN) based on the generative adversarial network (GAN) framework, incorporating a multi-resolution encoder and a dynamic graph convolutional feature extractor (DGCFE). This model was tailored to handle the complexity and variability of rapeseed canopy architectures across different growth stages.

(iii) We proposed a novel canopy architecture evaluation index, the silique efficiency index (SEI), to estimate yield potential for rapeseed populations. By comparing yield estimations derived from incomplete and complete point clouds, we demonstrated that reconstructing the complete architectural form of field-grown rapeseed significantly enhances yield prediction accuracy.

2. Methods

2.1 Generation of the training dataset for rapeseed population point cloud completion model

In order to develop the rapeseed population point cloud completion model, a virtual-real integration (VRI) simulation method combined with the occlusion point detection algorithm was proposed to generate a training dataset of the plot-level rapeseed population as shown in Fig.1. Multi-view videos of individual rapeseed plants at the seedling, bolting, flowering, and silique stages were captured using an unmanned aerial vehicle (UAV) (Fig. 1a). A sequence of images was extracted by sampling frames at regular time intervals, ensuring sufficient coverage of all external surfaces from different perspectives. The structure from motion (SfM) algorithm was applied to calculate the pose information for each image, and both the images and their corresponding pose information were input into the neural radiance field (NeRF) model to generate complete 3D models of individual rapeseed plants, including point clouds and triangle mesh model (Jiang et al., 2020).

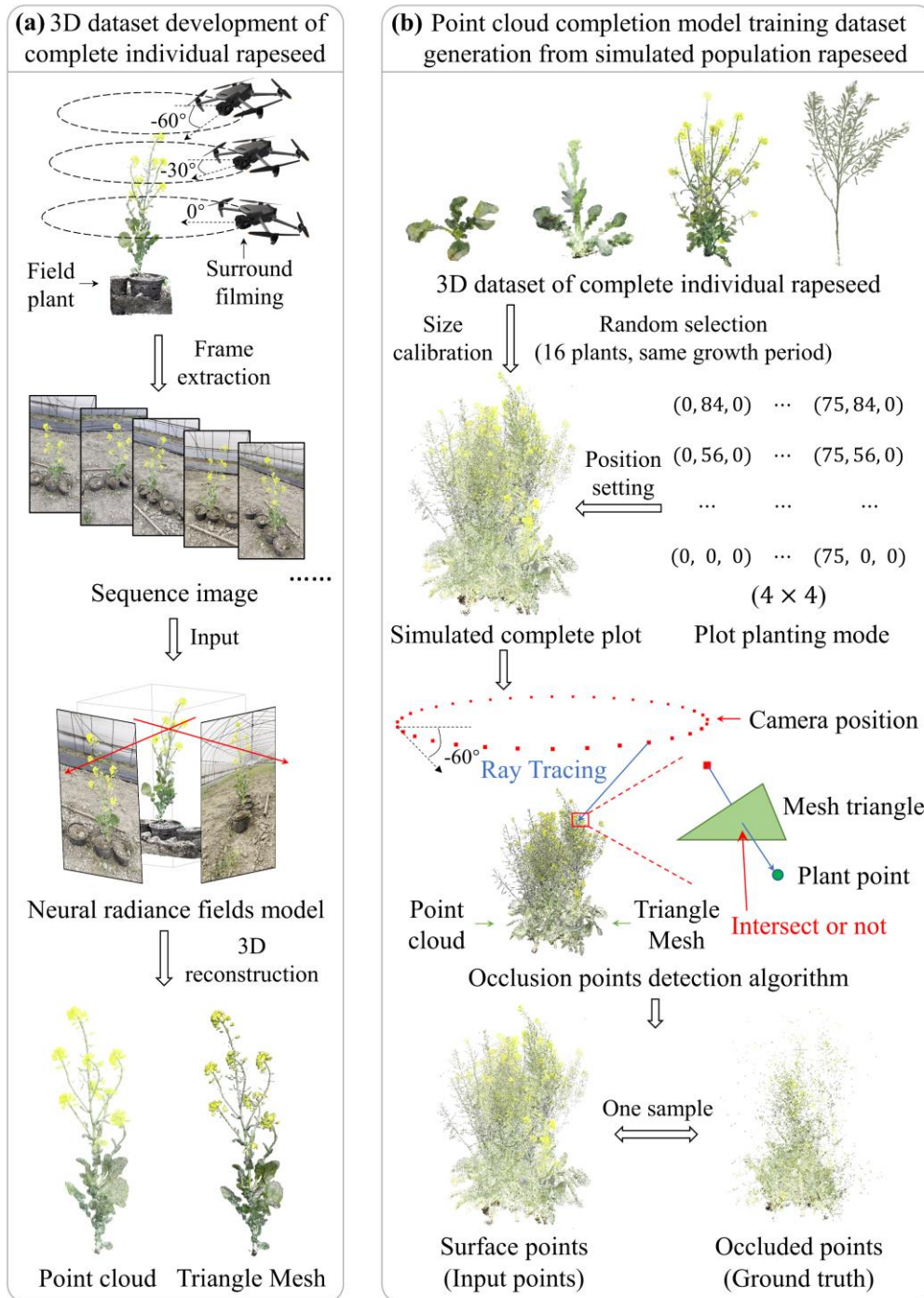


Fig. 1. Workflow of the training dataset generation for rapeseed population point cloud completion model, including (a) 3D dataset development for individual rapeseed plants and (b) annotated dataset generation for point cloud completion model.

Followed by the 3D reconstruction of individual plants, a plot layer with the plant number of 16, spacing of 25 cm, and row arrangement of 28 cm was designed to

simulate the real configuration of the field experiment as shown in Fig. 1b. The coordinates of each rapeseed plant within the simulated plot were then determined. Plants at the same growth stage were randomly selected from the individual rapeseed dataset, and the base of each plant's bounding box, corresponding to the point where the main stem intersects the root, was aligned with its designated coordinate within the simulated plot. This approach generated a complete population canopy architecture and was referred to the VRI method for 3D models simulation of rapeseed population.

To annotate the complete point cloud of rapeseed population as the surface point cloud and occluded point cloud for training the point cloud completion model, an occlusion point detection algorithm was developed based on ray tracing technology, building upon the simulated 3D models of rapeseed population. The algorithm distinguished surface points that can be reconstructed from multi-view imagery, from the occluded points that were entirely invisible due to the inter-plant occlusion within crop canopies. The pseudocode for the detailed process is described in Algorithm 1. It calculated the number of intersections between rays cast from each point to all camera positions and the triangular mesh model. The camera positions were determined by simulating the flight altitude, imaging angles, and the number of images at the real UAV campaign (Fig. 1b). Surface points, which are visible in at least one camera's field of view, were then designated as the input data of the point cloud completion model. Occluded points, which remained invisible across all viewpoints, served as the model's target output for completion.

Algorithm 1 occlusion point detection

Input: point cloud and triangle mesh of plant canopy, imaging coordinates.

Output: surface points, occluded points.

```
1: for each point in the plant point cloud:
2:     for each imaging point:
3:         for each triangle in the mesh model:
4:             if a ray from the plant point to the imaging point intersects with the
               triangle:
5:                 Increment intersection count by 1;
6:             end if
7:         end for
8:         if intersection count > 0:
9:             Increment occluded direction by 1;
10:        end if
11:    End for
12:    if occluded direction > total imaging points:
13:        Mark the point as completely occluded and unavailable from multi-view
               3D reconstruction;
14:    end if
15: end for
```

2.2 Network architecture

To address the highly variable and complex structural characteristics of rapeseed population canopy architectures across different growth stages, we designed a deep learning network called RP-PCN, which integrates the advantages of GANs and graph neural networks. A dynamic graph convolution mechanism was proposed to adaptively extract structural features corresponding to the different growth stages, enhancing the

model's ability to capture intricate morphological variations in rapeseed populations. As shown in Fig. 2b, RP-PCN was built upon a GAN framework, consisting of two primary components: the generator and the discriminator. The generator predicted the missing portions of the point cloud based on the incomplete input, while the discriminator evaluated the plausibility of the generated point cloud by distinguishing it from the ground truth data. To preserve plant structure during down-sampling, a sliding window approach was employed to segment large population point clouds into smaller, manageable blocks before processing (Fig. 2a). This strategy ensured structural integrity and enabled more effective learning of local and global canopy features.

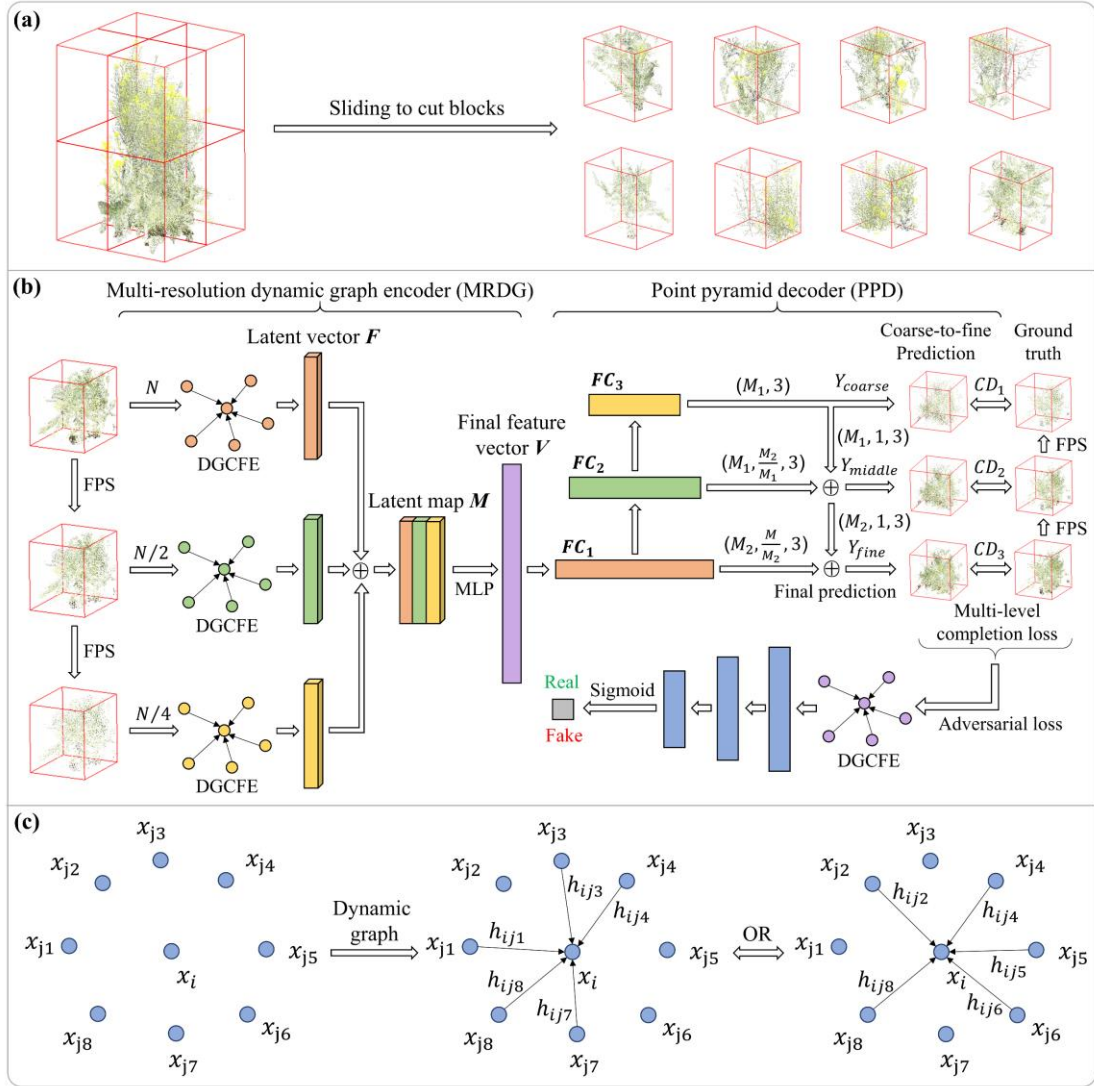


Fig. 2. Workflow of the rapeseed population point cloud completion network (RP-PCN). (a) The input rapeseed population point cloud is evenly divided into eight blocks using a sliding window strategy. (b) The RP-PCN adopts a generative adversarial network (GAN) framework, where the generator consists of a multi-resolution dynamic graph encoder (MRDG) and a point pyramid decoder (PPD). Before encoding, the input point cloud is down-sampled into three resolutions using iterative farthest point sampling (FPS). Feature extraction at each resolution is performed by the dynamic

graph convolutional feature extractor (DGCFE). (c) DGCFE can dynamically adjust the feature relationship between the center point and adjacent points.

2.2.1 Multi-resolution encoder

To accommodate the size variation and architectural complexity of rapeseed populations across different growth stages, a multi-resolution feature extraction strategy was conducted in this study. The input point cloud was down-sampled using iterative farthest point sampling (IFPS) to three resolutions, containing N (8192), $N/2$ (4096), and $N/4$ (2048) points, respectively (Charles et al., 2017). This hierarchical down-sampling mechanism enabled the network to capture both local and global features, ensuring that architectural details were preserved at multiple scales.

At each resolution level, the dynamic graph convolutional feature extractor (DGCFE) was applied through five layers, where each layer dynamically constructed local graphs to learn spatial relationships and high-level semantic features. Specifically, the feature dimensions of the extracted representations increased progressively from 64, 128, 256, 512, to 1024. To enhance feature aggregation, the output from the last four layers underwent a max pooling operation at each resolution, extracting the most salient feature representations. The pooled feature vectors were then concatenated across all layers, forming a 1920-dimensional latent vector (F). This comprehensive feature representation was subsequently aggregated into a final feature map (M), which integrated information from all resolutions to facilitate effective downstream point cloud completion.

2.2.2 Dynamic graph convolutional feature extractor

In the RP-PCN model, we designed a DGCFE to extract features from point clouds, leveraging its unique capability to dynamically update neighborhood relationships at each convolutional layer. Specifically, unlike traditional static graph architectures, the DGCFE recalculated k-nearest neighbor (k-NN) relationships based on the evolving feature space at each layer, allowing the network to flexibly adapt to variations in local geometry across layers and enhance spatial feature representation, as shown in Fig. 2c.

The DGCFE mechanism was built around the EdgeConv operation, which constructed edge features by considering both the center point and its neighbors (Wang et al., 2019). For a given center point p_i and one of its neighboring points p_j , EdgeConv computed an edge feature as follows:

$$h_{ij} = MLP([x_i, x_j - x_i]) \quad (1)$$

where x_i and x_j denoted the feature vectors of points p_i and p_j , respectively, and $[x_i, x_j - x_i]$ represented the concatenation of the center point's features with the relative position vector. A MLP was then applied to transform these concatenated features, capturing complex spatial relationships within each neighborhood.

After computing edge features h_{ij} for each point and its neighbors, a max pooling operation aggregated the edge features, resulting in a unique representation h_i for the center point p_i :

$$h_i = \max_{j=1, \dots, k}(h_{ij}) \quad (2)$$

This pooling operation emphasized the most significant features within each neighborhood, ensuring that the representation remained invariant to the ordering of

neighboring points. By repeating this process across multiple layers, the DGCFE progressively refined the neighborhood graph and captured detailed local structures in the point cloud data, yielding a robust and adaptive spatial feature representation. In this study, the size of k was set to 20.

2.2.3 Point pyramid decoder

The point pyramid decoder (PPD) was a crucial component of the RP-PCN model, responsible for decoding the high-dimensional feature vector into the missing point cloud. Operating as a hierarchical decoder, the PPD processed the input feature vector at multiple resolutions, ultimately reconstructing the occluded point cloud at three distinct scales. The PPD took the 5760-dimensional final feature vector V as input and generated the missing point cloud of size $M \times 3$, representing the shape of the missing region. The PPD operated as a hierarchical decoder, processing features at different resolutions. The input feature vector was passed through multiple stages to progressively refine the point cloud completion. Initially, the feature vector V was passed through the fully connected layers, resulting in three feature layers: FC_3 (512 neurons), FC_2 (1024 neurons), FC_1 (1920 neurons). Each of these layers was responsible for predicting point cloud structures at different resolutions. At the deepest layer, FC_3 predicted the primary center points Y_{coarse} , which had a size of $M_1 \times 3$. These primary center points served as the foundation for further refinement. Then, FC_2 predicted the relative coordinates of secondary center points Y_{middle} . Each point in Y_{coarse} acted as a center point to generate M_2 points of Y_{middle} , refining the structure of the predicted point cloud. The process involved "Expand" and "Add" operations,

where the size of Y_{middle} became $M_2 \times 3$. Finally, the detailed point cloud Y_{fine} was predicted by FC_1 resulting in the final high-resolution prediction. The generation of Y_{fine} followed the same principle as Y_{middle} but focused on finer structural details, as illustrated in Fig. 2b. The size of Y_{fine} is $M \times 3$, and it was designed to closely match the feature points sampled from the ground truth. By leveraging this hierarchical structure, high-level features extracted from the initial coarse layers influenced the generation of detailed features, thereby minimizing distortion and preserving the fine geometric details of the original missing point cloud. Here, the values of M , M_1 , M_2 were set to 8192, 2048, 4096, respectively.

2.3 Loss function

The loss function played an essential role in training the RP-PCN model, guiding the optimization of both the feature extraction and point cloud completion processes. It consisted of two key components: multi-stage completion loss and adversarial loss. The completion loss measured the difference between the ground truth missing point cloud Y_{GT} and the predicted point cloud, while the adversarial loss optimized the MRDG and PPD to ensure that the predicted output appeared more realistic. The size of Y_{GT} was $M \times 3$, which matched Y_{fine} . The commonly used chamfer distance (CD), widely applied in point cloud completion research (Wu et al., 2021), was adopted as the model's loss function, which was calculated as follows:

$$d_{CD}(S_1, S_2) = \frac{1}{S_1} \sum_{x \in S_1} \min_{y \in S_2} \|x - y\|_2^2 + \frac{1}{S_2} \sum_{y \in S_2} \min_{x \in S_1} \|y - x\|_2^2 \quad (3)$$

where S_1 and S_2 represented two sets of 3D point clouds. CD in Equation (3) measured the average nearest squared distance between the predicted point cloud S_1

and the ground truth point cloud S_2 . Since the PPD predicted three point clouds at different resolutions, the multi-stage completion loss was formulated as follows:

$$L_{com} = d_{CD1}(Y_{fine}, Y_{GT}) + \alpha d_{CD2}(Y_{middle}, Y'_{GT}) + 2\alpha d_{CD3}(Y_{coarse}, Y''_{GT}) \quad (4)$$

where d_{CD1} , d_{CD2} and d_{CD3} represented the CD at different resolution levels, weighted by the hyperparameter α . The weighting parameter α was progressively updated as the number of training epochs increased. The first term calculated the squared distance between the detailed points Y_{fine} and the ground truth of the missing region Y_{GT} . The second and third terms calculated the squared distance between the primary center points Y_{coarse} and secondary center points Y_{middle} and their corresponding subsampled ground truth Y''_{GT} , Y'_{GT} , respectively. The subsampled ground truth Y''_{GT} and Y'_{GT} were obtained by applying IFPS to extract representative feature points from the missing region and were of sizes $M_1 \times 3$ and $M_2 \times 3$, respectively.

The adversarial loss was inspired by GANs. The generator function was defined as $F(\cdot) = PPD(MRDG(\cdot))$, where $F: \mathcal{X} \rightarrow \mathcal{Y}'$ mapped the partial input \mathcal{X} to the predicted missing region \mathcal{Y}' . The discriminator $D(\cdot)$ attempted to distinguish between the predicted missing region \mathcal{Y}' and the real missing region \mathcal{Y} . The discriminator incorporated both a DGCFE module and an MLP network to compare the predicted point clouds with the ground truth. The structure of the DGCFE remained consistent with its implementation in the MRDG. The MLP network consisted of sequential layers with dimensions [64 – 64 – 128 – 256], where max pooling was applied to the outputs from the last three layers to obtain a compact feature representation. These pooled

feature vectors were concatenated to form a 448-dimensional latent vector, which was subsequently passed through fully connected layers [256, 128, 16, 1], and a sigmoid classifier to generate the final discrimination result. The adversarial loss was computed based on the discriminator's performance as follows:

$$L_{adv} = \sum_{1 \leq i \leq S} \log(D(y_i)) + \sum_{1 \leq i \leq S} \log(1 - D(F(x_i))) \quad (5)$$

where $x_i \in \mathcal{X}$, $y_i \in \mathcal{Y}$, $i = 1, 2, \dots, S$, with S representing the dataset size. Both $F()$ and $D()$ were jointly optimized using alternating Adam updates during training.

The final loss function, combining the multi-resolution completion loss and adversarial loss, was formulated as:

$$L = \lambda_{com}L_{com} + \lambda_{adv}L_{adv} \quad (6)$$

where λ_{com} and λ_{adv} were weight hyperparameters satisfying $\lambda_{com} + \lambda_{adv} = 1$. In this study, λ_{com} was set to 0.9.

3. Experiments

3.1 Experimental design and data acquisition

For data acquisition, two distinct experimental setups were designed: a field experiment and a greenhouse potted plant experiment. The field experiment aimed to capture 3D models of individual plants and surface point clouds of rapeseed population under field growth conditions. The potted plant experiment was designed to assess the differences in canopy architecture between plants grown in a controlled environment and those grown in the field. The field experiments were performed at the experimental field of the Jiaying Academy of Agricultural Sciences, Zhejiang Province, China (120°41'39"E, 30°51'14"N). A total of 300 rapeseed germplasm resources were

cultivated, with each accession planted in three replicates, resulting in 900 experimental plots (Fig. 3). Each plot contained 16 plants, arranged with a row spacing of 28 cm and a plant spacing of 25 cm. To ensure uniform growth conditions, water and nutrient management were optimized throughout the study period without any special treatments. In addition, four rapeseed accessions with distinct plant architectures were randomly selected for potted cultivation in a greenhouse at the Agricultural Experimental Station of Zhejiang University, Hangzhou, China (120°4'46"E, 30°18'31"N), and each accession was grown in 16 pots.

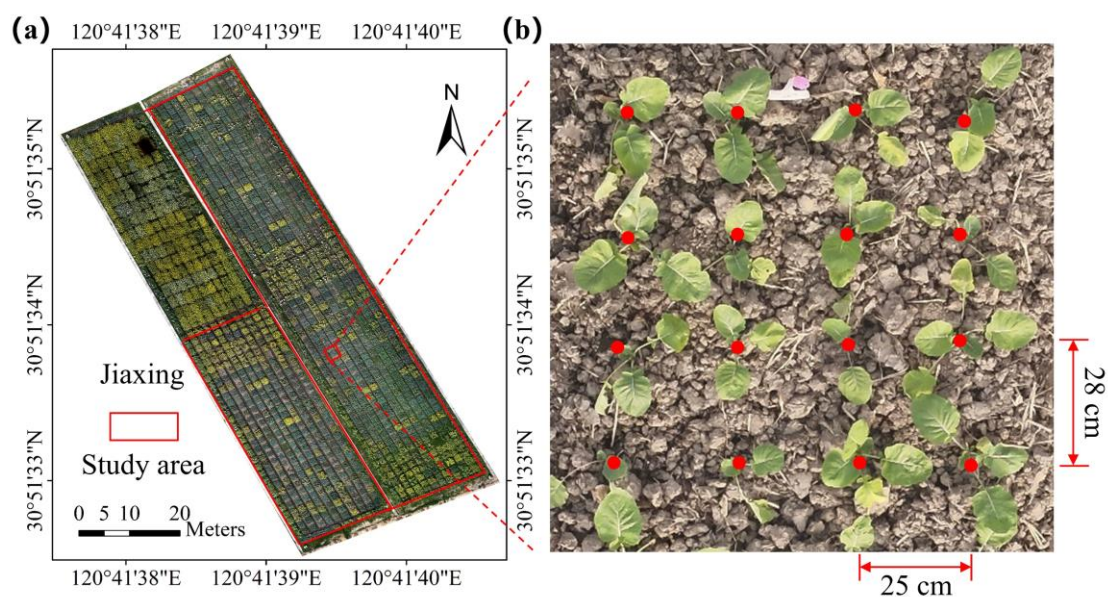


Fig. 3. Location of the experimental field (a) in Jiaxing, Zhejiang province, China with (b) the rapeseed plant layout within a plot. Each plot contains 16 rapeseed plants with the spacing of 28×25 cm.

For field-grown individual plants, one plant was randomly selected from the center of each of 100 plots (randomly chosen from one replicate of the 300 accessions) at four

key growth stages, seedling, bolting, flowering, and silique, yielding a total of 400 potted plants (100 per stage). To avoid edge effects, only plants from the central area of each plot were selected for sampling. For individual plant imaging, a DJI Mavic 3T UAV (DJI, Shenzhen, China) was used to capture high-resolution videos at 30 frames per second with the size of 3840×2160 pixels. To ensure full coverage of the plant surface, the UAV circled each potted plant three times at camera inclination angles of 0° , 30° , and 60° relative to the horizontal plane. A preliminary experiment confirmed that this strategy enabled the reconstruction of a complete and accurate 3D models of the rapeseed. The same approach was used to capture the 3D models of the potted plants.

For field-level rapeseed populations, UAV oblique imaging campaign with a single circular flight path was performed to acquire the multi-view images of each plot at the four growth stages. It is hypothesized that only canopy surface information was obtained due to the severe occlusions within the canopy. During each campaign, UAV maintained a -60° viewing angle and a 5-meter distance from the plot center. Images were acquired every 10° along the circle, resulting in 36 images per plot, each with the image size of 8000×6000 pixels. Thirty-two plots were randomly selected from the 300 rapeseed accessions that were not subjected to destructive sampling, for UAV imaging. These plots were used to test the similarity between the simulated rapeseed population surface point clouds and the actual field data, as well as for yield prediction using data from the silique stage. Additionally, five plots were selected for destructive sampling. After UAV imaging, the spatial relative positions of all plants within each plot were recorded. The plants were then excavated from the field plots, transplanted

into pots, and individually scanned using UAV video for further testing of the RP-PCN model's ability to complete point clouds for field-grown rapeseed populations.

3.2 Dataset preparation

To ensure accurate annotation of surface and occluded points, it was essential to obtain 3D models, including both the triangular mesh and corresponding point cloud, during the reconstruction process. After evaluating several NeRF-based models in terms of mesh quality and training efficiency, Instant-NGP was selected as the 3D reconstruction algorithm in this study due to its favorable balance between the signal-to-noise ratio and computational speed (Müller et al., 2022). The pose information for each frame was computed using COLMAP 3.9.1 (with CUDA support), based on sequential images extracted at a rate of 3 frames per second from UAV videos. Finally, 400 complete 3D models of individual plants were reconstructed, representing 100 plants at four growth stages. In addition, UAV multi-view images of plot-level rapeseed populations were also processed using COLMAP to estimate camera poses, which were then used as the input of the Instant-NGP model to reconstruct the 3D point cloud of the canopy surface for each plot.

To generate the simulated dataset of rapeseed population 3D models with the VRI method, the planting configuration with the coordinates of 16 plants within a single plot were predefined as follows:

$$\begin{bmatrix} (0,84,0) & (25,84,0) & (50,84,0) & (75,84,0) \\ (0,56,0) & (25,56,0) & (50,56,0) & (75,56,0) \\ (0,28,0) & (25,28,0) & (50,28,0) & (75,28,0) \\ (0,0,0) & (25,0,0) & (50,0,0) & (75,0,0) \end{bmatrix} \quad (7)$$

The VRI method was applied 1,000 times for each growth stage to generate diverse

rapeseed population canopy architectures. Using the UAV imaging parameters and the simulated plot center coordinates $(37.5, 42, 0)$, the corresponding virtual camera positions were calculated. After applying the occlusion detection algorithm to each simulated plot, a total of 4,000 training samples were generated for point cloud completion model. Each sample was divided into eight sub-blocks using a sliding window, and the dataset was subsequently split into 80% for training and 20% for validation.

For the five destructively sampled field plots, all individual plant videos were processed using the same 3D reconstruction pipeline to obtain complete canopy models. They were then assembled by VRI method using the recorded relative positions of each plant, and the ground truth of the complete point cloud for five plot-level rapeseed populations were obtained.

3.3 Evaluation of similarity between simulated and real point clouds

The three-dimensional structural similarity index (SSIM3D) was utilized to assess the similarity between the surface point clouds from UAV multi-view images and simulated population point clouds (Alexiou and Ebrahimi, 2020). The calculation formula is as follows:

$$SSIM3D(X, Y) = \frac{1}{N} \sum_{p=1}^N \frac{|F_X(q) - F_Y(p)|}{\max(|F_X(q)|, |F_Y(p)|) + \varepsilon} \quad (8)$$

where X and Y represent two sets of 3D point clouds, $F_X(q)$ and $F_Y(p)$ denote the feature values of points q and p , respectively, and N is the number of points in the point cloud. The term ε is a small value to prevent division by zero.

For each of the 32 real field plots, SSIM3D values were calculated against 1000 candidate simulated plots, and the highest similarity score was retained as the final evaluation metric for each plot. To ensure a fair and meaningful comparison, the simulated point clouds first underwent occlusion point detection, and the resulting surface point clouds were then used as the basis for similarity evaluation. This step ensured that only the structurally observable regions corresponding to UAV-derived reconstructions were compared, thereby reflecting the fidelity of the simulated canopy to real-world field conditions. The overall similarity score for each simulation strategy was computed by averaging the highest SSIM3D values across all 32 plots. In addition to the proposed virtual-real integrated simulation approach, two conventional methods based on individual plant replication were evaluated: one using potted plant models and the other using field-grown individuals. Given the morphological divergence between these plant types and the substantial structural variation across different growth stages, comparisons were conducted separately for each stage. This design enabled a comprehensive, stage-specific assessment of each method's ability to reproduce realistic canopy architectures under field conditions.

3.4 Network training, validation and testing

The training and validation of the RP-PCN model were conducted on the simulated dataset of rapeseed populations, which included annotated surface and occluded point clouds. The proposed network was implemented using PyTorch and trained on a server equipped with an Intel i9-10900K CPU and an Nvidia RTX 3090 GPU, running Ubuntu 20.04. The model was optimized using the Adam optimizer with an initial learning rate

of 0.0001 and a batch size of 8. Due to the lack of publicly available datasets for training plant population point cloud completion model, the RP-PCN weights were initialized randomly rather than being pre-trained through transfer learning on an existing dataset. Training continued until the loss function dropped below 0.1 or a maximum of 200 epochs was reached. Batch normalization (BN) and ReLU activation were applied to the MRDG and discriminator, while the PPD utilized only ReLU activation, except for the final output layer. To balance different loss components during training, the weighting parameter α was dynamically adjusted based on the training epoch: 0.01 for the first 30 epochs, 0.05 from epochs 30 to 80, and 0.1 after epoch 80. Every 10 epochs, the model's performance was evaluated on the validation dataset by computing the loss value, and if the loss decreased, the model weights were updated. This periodic evaluation ensured effective monitoring of model generalization and prevented overfitting.

After training, the RP-PCN was applied to the surface point clouds of rapeseed population reconstructed from UAV imagery in five destructively sampled field plots. The occluded point clouds were then predicted using the trained model and subsequently merged with the input data to obtain the complete 3D reconstruction of rapeseed populations. The prediction results were then compared with the ground truth of complete point cloud for five plot-level rapeseed populations to test the model's performance (Fig. 4).

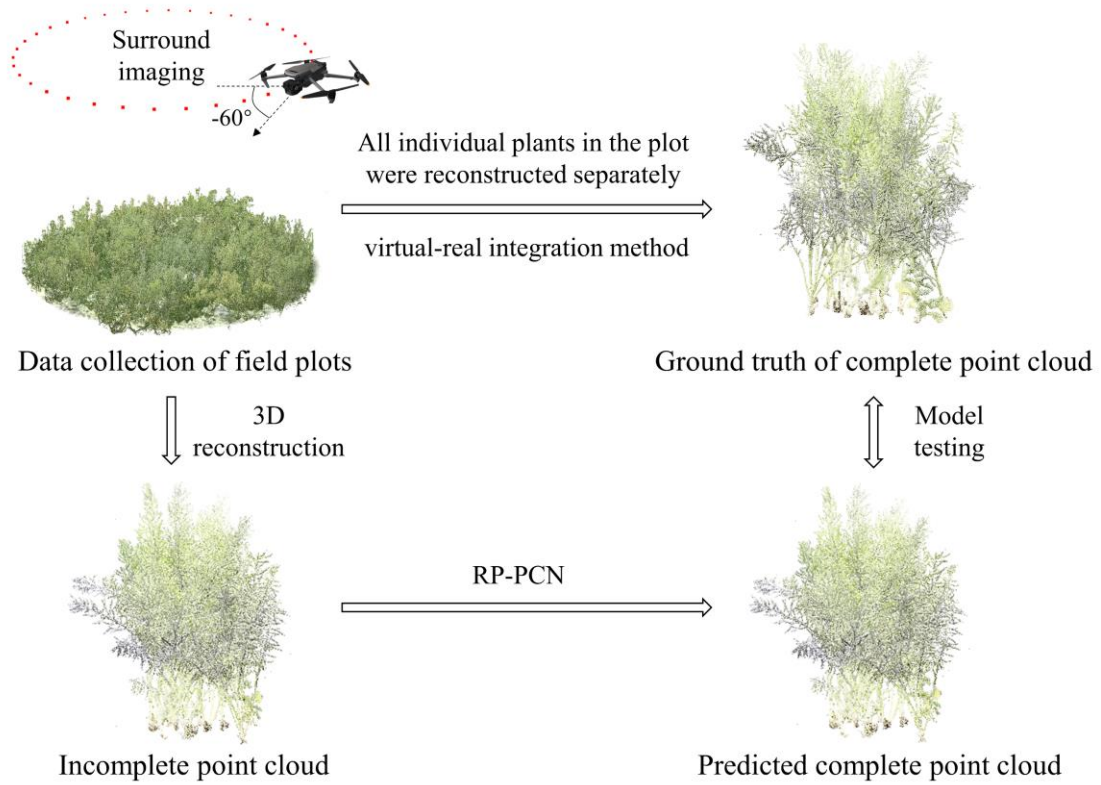


Fig. 4. Model testing pipeline of the rapeseed population point cloud completion network (RP-PCN) using field plot data.

3.5 Ablation study and hyper-parameter analysis

To investigate the contribution of key network components, ablation studies were conducted by modifying the MRDG and DGCFE. Specifically, two experiments were designed: one replacing the multi-resolution encoder with a single-resolution encoder to evaluate the effect of multi-scale feature extraction, and another substituting the graph-based feature extractor with a MLP to assess the impact of dynamic graph convolution on point cloud feature learning. These modifications were tested under identical conditions to examine their influence on point cloud completion accuracy.

In addition, we conducted a sensitivity analysis on four hyper-parameters: (i) the number of nearest neighbors (k) in dynamic graph convolution, tested with values

{8, 10, 12, 16, 20, 24, 28, 32}; (ii) the input (N) and output (M) point cloud sizes, varied across {2048, 4096, 8192, 16384}; and (iii) the number of layers (O) in the MRDG, set to {4, 5, 6, 7}. Based on prior research, the first five layers were set to {64, 128, 256, 512, 1024}. For deeper configurations with six and seven layers, the additional layers were set to 2048 and 4096, respectively, to further enhance feature extraction capacity. Each parameter was varied independently while keeping the others constant to isolate its effect on model performance.

3.6 Comparison analysis

To further evaluate the effectiveness of RP-PCN, we benchmarked it against several state-of-the-art point cloud completion models, including PF-Net, GRNet, and PoinTr (Huang et al., 2020; Xie et al., 2020; Yu et al., 2021). These models were selected as they represent distinct paradigms in point cloud completion. PF-Net, a lightweight model, utilizes a GAN-based architecture with MLP-based feature extraction to generate missing regions. GRNet employs a deep residual network structure, inspired by ResNet (He et al., 2016), to enhance precision through hierarchical feature learning. In contrast, PoinTr incorporates a transformer-based architecture, achieving high accuracy but at the cost of increased computational complexity (Vaswani et al., 2017). All models were trained and tested under identical conditions, ensuring a fair comparison. Performance was evaluated based on visual inspection, CD, and computational efficiency, allowing for a comprehensive assessment of reconstruction quality and model efficiency.

3.7 RP-PCN for yield estimation

To evaluate the practical value of RP-PCN in agronomic applications, this experiment aimed to assess whether point cloud completion enhances the accuracy of rapeseed yield estimation. The morphological architecture of rapeseed siliques is closely related to yield. Therefore, a novel index, the silique efficiency index (SEI), was introduced based on the complete point cloud data to quantify the silique volume relative to the ground area of the plot (Fig. 5), providing a more comprehensive evaluation of the relationship between silique morphology and yield. This index was calculated by first applying a rapeseed organ segmentation model PST to separate the siliques from the overall population point cloud, followed by voxelization to compute the total silique volume (Du et al., 2023). The SEI was then determined by dividing the silique volume by the actual ground area of the plot, as represented in Equation (9):

$$\text{Silique efficiency index} = \text{silique volume} / \text{plane area} \quad (9)$$

To validate the SEI's relationship with yield, 32 non-destructive sampling plots were selected as observation targets. Once the siliques reached full maturity, manual threshing was performed, followed by drying and weighing to obtain the actual yield of each plot. The SEI was calculated for both complete and incomplete point clouds, and their respective correlations with yield were analyzed. The correlation analysis was evaluated using the R^2 , which was calculated as follows:

$$R^2 = 1 - \frac{\sum_{i=1}^n (y_i - \hat{y}_i)^2}{\sum_{i=1}^n (y_i - \bar{y}_i)^2} \quad (10)$$

where y_i represents the observed yield values, \hat{y}_i represents the predicted yield values, and \bar{y}_i is the mean of the observed yield values, n is number of samples.

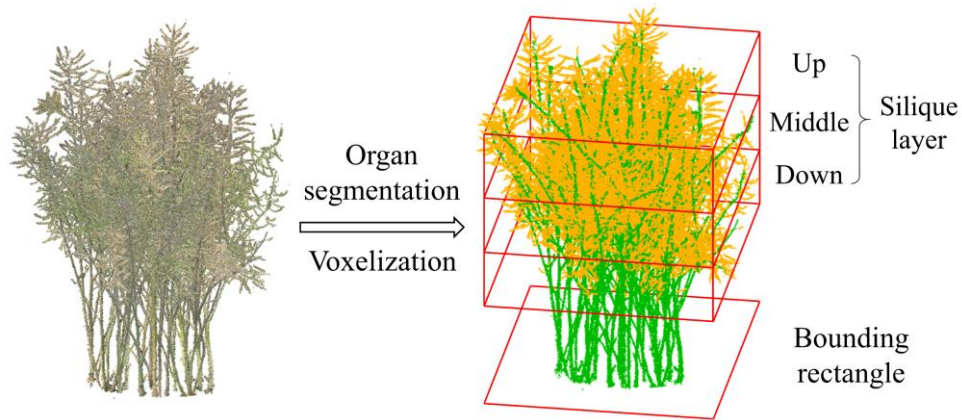


Fig. 5. Schematic illustration of stratified analysis of silique structures within rapeseed canopies.

4. Results

4.1 Structural similarity between simulated and real point clouds of rapeseed populations

Fig. 6 presents a quantitative comparison of the structural similarity between simulated and real rapeseed population point clouds across four key growth stages. The proposed VRI method combined with the occlusion point detection achieved the highest SSIM3D values of 0.95, 0.94, 0.91, and 0.89 for the seedling, bolting, flowering, and silique stages, respectively, indicating its strong capacity to reproduce realistic canopy architectures under field conditions. In contrast, the simple repetition of individual field-grown plants yielded moderate similarity scores, with the SSIM3D values decreasing from 0.85 at the seedling stage to 0.72 at the silique stage. The repetition of potted plants performed the worst, with similarity scores dropping from 0.68 to 0.55 across the same stages. Overall, the high and stable similarity scores achieved by the VRI method across all stages demonstrate its superiority in producing realistic and structurally accurate rapeseed canopy point clouds, while traditional

population simulation strategies failed to capture complex features of canopy structures, especially at the later growth stages.

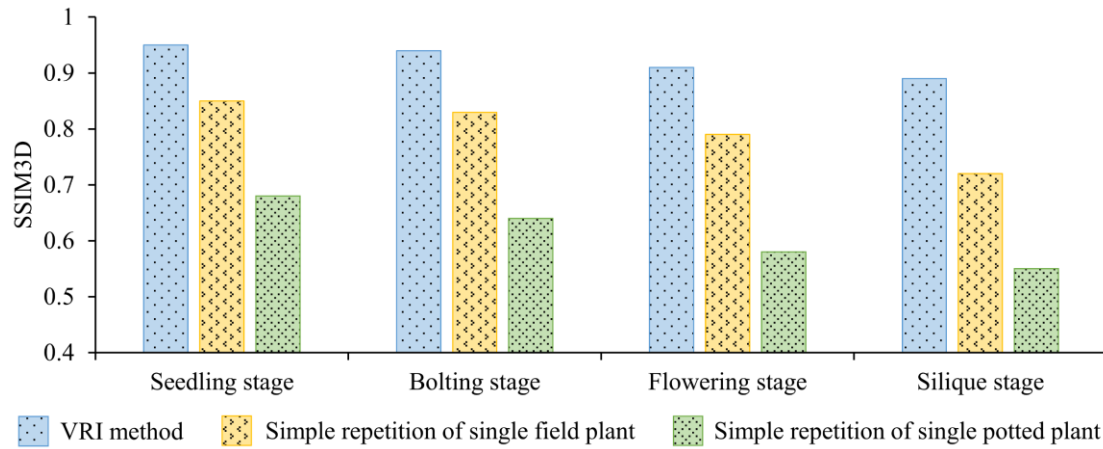


Fig. 6. Evaluation of canopy similarity between simulated and actual field rapeseed populations at four growth stages using the three-dimensional structural similarity index (SSIM3D). The comparison includes three simulation strategies: (i) simple repetition of individual potted plant, (ii) simple repetition of individual field plant, and (iii) the proposed virtual-real integration (VRI) method.

4.2 Evaluation of RP-PCN performance

The RP-PCN model demonstrated robust performance in reconstructing rapeseed canopy structures across four growth stages, including seedling, bolting, flowering, and silique stages. As illustrated in Fig. 7, the model successfully reconstructed both external and internal canopy architectures, with slices along the X, Y, and Z planes highlighting the internal details of the completed point clouds. Enlarged regions further emphasized the model's ability to recover occluded areas. The full point cloud results, providing a comprehensive view of the reconstructed canopy, are provided in Appendix A.1. At the seedling stage, the model effectively reconstructed sparse input data, achieving accurate point cloud generation across all axes. As complexity increased

during the bolting, flowering, and silique stages, the model continued to demonstrate high accuracy, handling intricate canopy structures and recovering 3D architectural details with the minimal deviation.

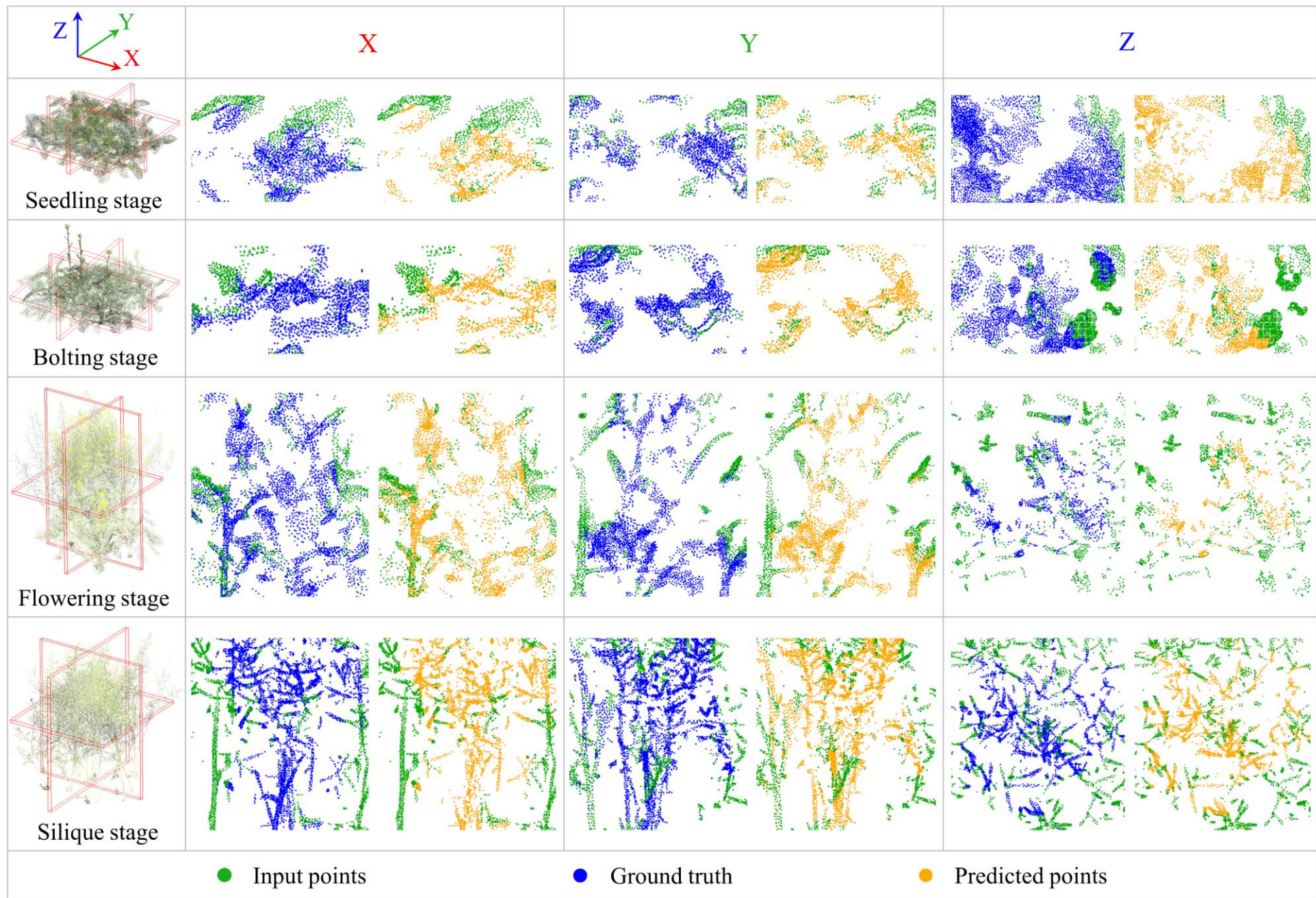


Fig. 7. Visualization of the complete point cloud at four different growth stages generated by the rapeseed population point cloud completion network (RP-PCN). Examples of the complete point cloud extracted from the X, Y, and Z planes are presented with the input points, ground truth and predicted points denoted by green, blue, and orange dots, respectively.

The model's performance was further validated by applying it to incomplete point clouds collected from field-grown rapeseed populations, as shown in Fig. 8. The comparison between the incomplete input data and the RP-PCN-generated completed point clouds illustrates the model's effectiveness in restoring missing plant structures, especially in the silique and branch areas. The predicted point clouds (shown in orange) seamlessly fill the gaps in the input data (shown in green), confirming the model's ability to address occlusions and recover detailed canopy morphology in field-collected datasets.

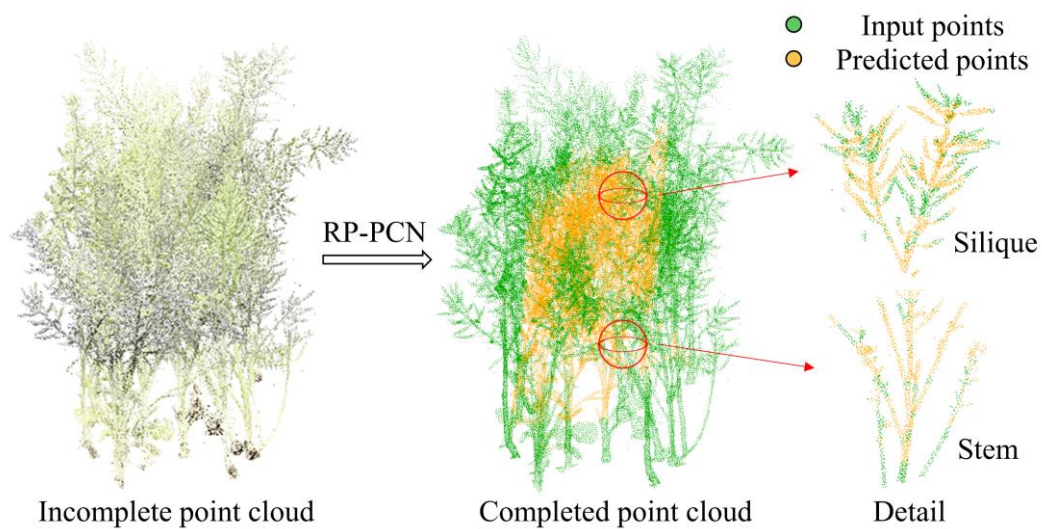


Fig. 8. Visualization and detailed results of the rapeseed population point cloud completion network (RP-PCN) applied to the completion of point clouds for field-grown rapeseed plot.

Quantitative evaluations across five different rapeseed accessions, presented in Table 1, show that the RP-PCN achieved consistent performance across all accessions with similar results for both CD and SSIM3D. The average CD value was 4.42 cm, with *Narowal-D1* showing the lowest CD value at 4.35 cm, while *Kurander* and *ZAAS-M5*

exhibited slightly higher values at 4.46 cm and 4.51 cm, respectively. For SSIM3D, the model demonstrated high structural fidelity across all accessions, with average scores close to 0.9, indicating reliable completion performance. *ZAAS-M5* and *Kurander* showed slightly lower SSIM3D values compared to other accessions, with *Narowal-D1* achieving the highest at 0.91. These results demonstrate that while performance is consistently strong across all accessions, there are slight variations, with *Narowal-D1* consistently performing slightly better in both CD and SSIM3D compared to the others.

Table 1. Quantitative evaluation of the rapeseed population point cloud completion network (RP-PCN) across five rapeseed accessions using chamfer distance (CD) and three-dimensional structural similarity index (SSIM3D).

| Rapeseed accessions | <i>Narowal-D1</i> | <i>ZAAS-M5</i> | <i>Kurander</i> | <i>Furax</i> | <i>Marasaki</i> | Mean |
|---------------------|-------------------|----------------|-----------------|--------------|-----------------|------|
| CD / cm | 4.35 | 4.51 | 4.46 | 4.33 | 4.43 | 4.42 |
| SSIM3D | 0.91 | 0.86 | 0.88 | 0.89 | 0.89 | 0.89 |

4.3 Comparison with other models

Fig. 9 presents the comparison results of rapeseed point cloud completion across different models. The RP-PCN consistently provided the highest accuracy, capturing fine canopy and silique features with high fidelity, and producing 3D reconstructions that closely matched the ground truth. In contrast, PF-Net and GRNet struggled to reconstruct detailed branch architectures and siliques, with considerable discrepancies between the predicted and ground truth point clouds. Although the PoinTr model

achieved relatively better results in some stages, it faced difficulties in complex canopy formations, often missing critical architectural elements.

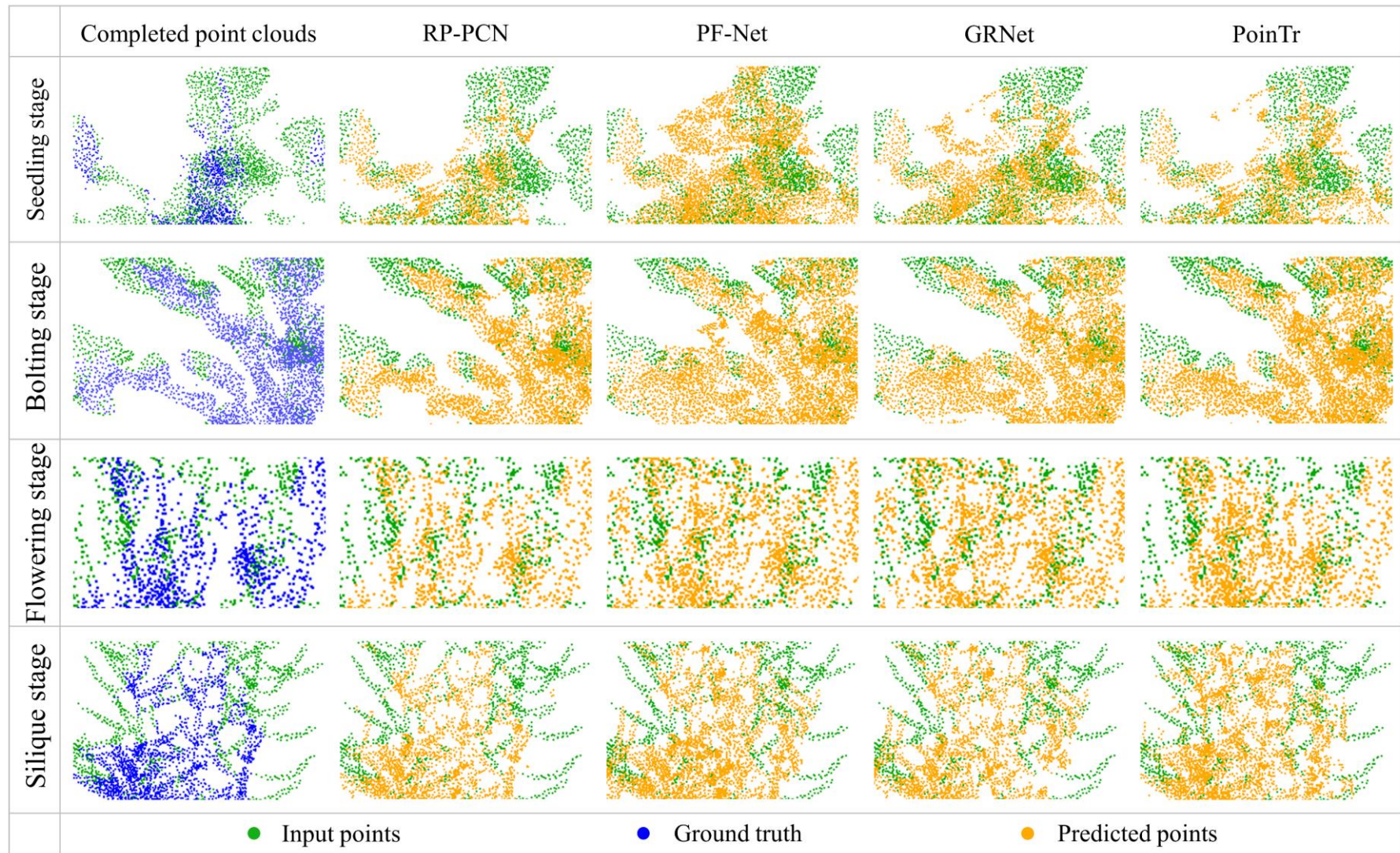


Fig. 9. Visualization of the complete point clouds of rapeseed populations at four different growth stages generated by RP-PCN, PF-Net, GRNet, and PoinTr.

Input points, ground truth, and predicted points in the completed point cloud are denoted as green, blue, and orange dots, respectively.

Quantitative evaluations further confirmed these observations (Fig. 10a). The RP-PCN model outperformed all other models across all stages, with CD values of 3.35 cm, 3.46 cm, 4.32 cm, and 4.51 cm for the seedling, bolting, flowering, and silique stages, respectively, resulting in an overall average CD of 4.05 cm. In contrast, PF-Net and GRNet exhibited high CD values, indicating weaker reconstruction abilities, particularly in later growth stages. During the silique stage, CD values for PF-Net and GRNet were 11.98 cm and 8.34 cm, respectively. Although PoinTr achieved improved accuracy, it still yielded higher CD values than RP-PCN.

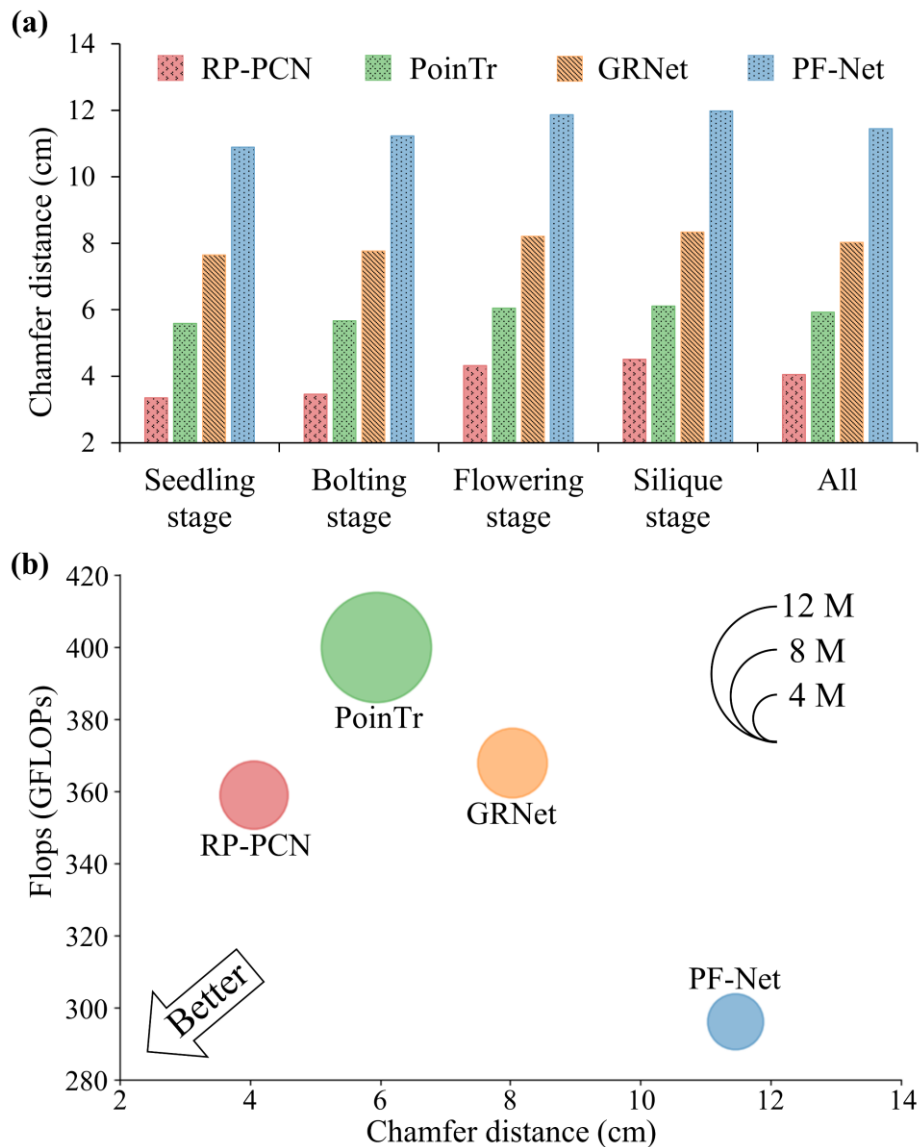


Fig. 10. Quantitative and computational comparison of the rapeseed population point cloud completion network (RP-PCN) with other point cloud completion algorithms. (a) Chamfer distance (CD) metrics for the models RP-PCN, PF-Net, PoinTr, and GRNet across different growth stages. (b) Performance comparison of the models in terms of CD, floating-point operations per second (FLOPs), and model size.

In addition to accuracy, the computational efficiency and model size of each algorithm were evaluated (Fig. 10b). RP-PCN effectively balanced high accuracy with computational efficiency, making it a suitable choice for large-scale, high-throughput field applications. In comparison, PF-Net was computationally efficient due to its simplicity, but its poor performance in point cloud completion limited its application in high-precision tasks. PoinTr and GRNet, while achieving better accuracy, incurred substantial computational costs and had large model sizes. Specifically, PoinTr required about 420 giga floating point operations per second (GFLOPs), leading to longer inference times.

4.4 Rapeseed yield estimation

The SEI values derived from complete population point clouds exhibited a higher correlation with rapeseed yield compared to those derived from incomplete point clouds as shown in Fig. 11. Regression analysis revealed that SEI calculated from the complete point cloud data achieved the R^2 of 0.90, significantly improving the yield estimation accuracy, compared to 0.81 for incomplete point cloud data. This improvement highlights the importance of the RP-PCN model in enhancing the precision of yield prediction. In addition, the SEI derived from the middle silique zone demonstrated the

highest correlation with yield, with R^2 values increasing from 0.69 to 0.79, further underscoring the crucial role of complete point clouds in refining yield estimation. This finding is consistent with previous research, which indicates that siliques from the middle canopy layers contribute most significantly to yield (Lin et al., 2024). In contrast, the SEI calculated from the lower and upper silique regions showed lower R^2 values, indicating their relatively minor contribution to the overall yield, possibly influenced by environmental and genetic factors.

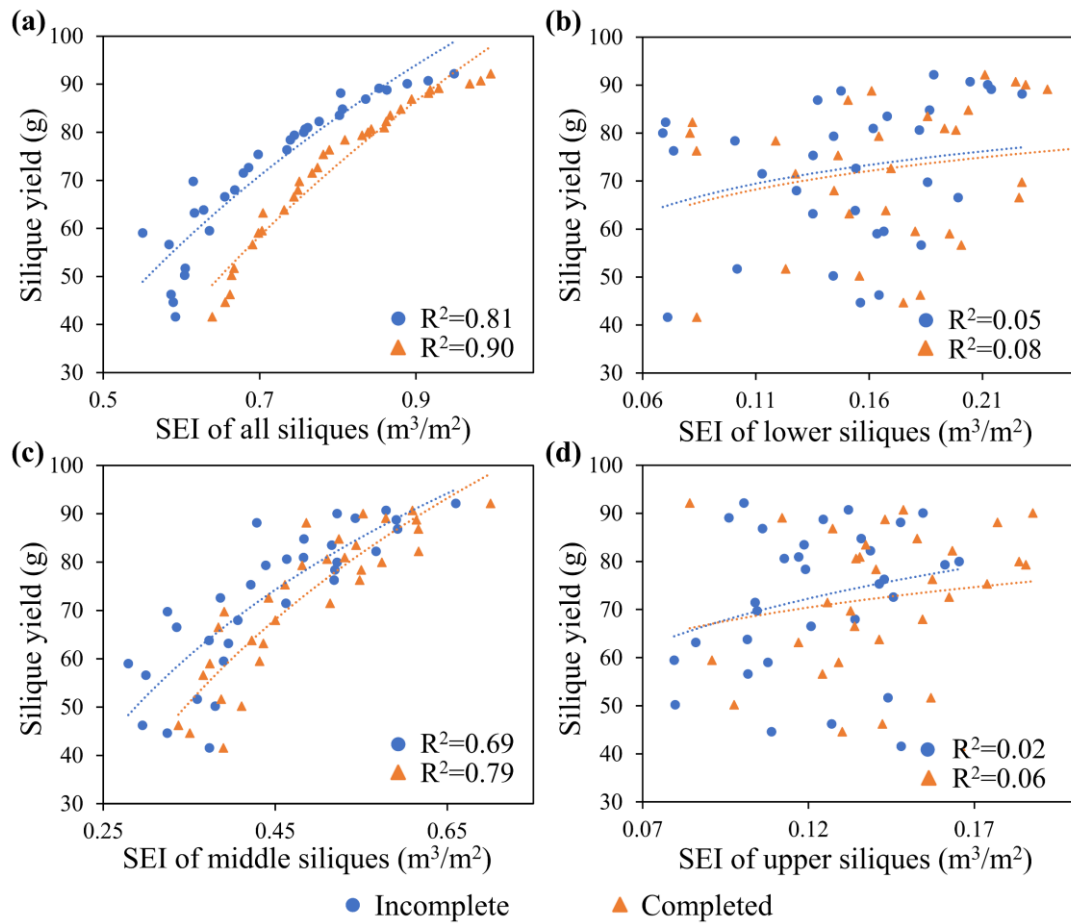


Fig. 11. Regression analysis between silique efficiency index (SEI) and silique yield based on complete and incomplete point clouds. (a) SEI derived from all silique layers.

(b) SEI from the lower layer. (c) SEI from the middle layer. (d) SEI from the upper layer.

5. Discussion

5.1 Importance of the high-quality annotated data for modeling

The quality of the training dataset is a critical factor for the performance of deep learning models. A high-quality dataset must be representative, encompassing a broad spectrum of target scenarios, sufficiently diverse to reflect the range of states and conditions present in the target, and must feature precise annotations to prevent the model from learning biased or erroneous patterns (Paullada et al., 2021). In constructing the rapeseed population point cloud completion dataset, we firstly proposed a novel simulation method, referred to as VRI, which produced more realistic simulation results by extracting dynamic nature of rapeseed canopy architectures throughout growth compared to the conventional approach of replicating individual plant data. During the seedling stage, the canopy architectures of different individuals within the same accession are relatively uniform, making traditional replication methods reasonably effective (Sun et al., 2021). However, as plants enter the flowering and silique stages, even individuals of the same accession exhibit substantial variability in canopy architecture, and simple replication of individual plants fails to capture this true diversity at the population level. Moreover, the proposed occlusion point detection algorithm successfully identified actual occlusion points from the simulated complete canopy point clouds, which should be included for model learning in the training dataset. This approach follows the principles of multi-view 3D reconstruction, where UAV-

based imaging typically captures only surface information, while internal structures remain occluded and unreconstructed. Existing methods often create datasets by randomly clipping sections from complete point clouds, which results in many surface points being incorrectly included as targets for completion and finally reducing overall accuracy (Chen et al., 2023, Huang et al., 2020). By focusing on occluded points, our method ensures the training dataset better represents real-world conditions, improving model performance.

5.2 Influence of hyper-parameters, DGCFE and MRDG on RP-PCN

The results from the ablation study highlight the crucial roles that both the DGCFE and MRDG modules play in enhancing point cloud completion performance in RP-PCN (Fig. 12). These findings align with the dynamic and complex nature of rapeseed canopy growth, where structural variations arise at different growth stages. During the early stages of growth, rapeseed canopies exhibit relatively simple geometric features, which require effective local feature extraction for accurate modeling. The DGCFE module, which specializes in this task, significantly enhances the model's ability to recover fine details, particularly in sparse or irregular canopy structures. As growth progresses, the canopy's structural complexity increases, necessitating the MRDG module to model hierarchical relationships and capture broader architectural features that emerge during later stages. The RP-PCN's ability to dynamically adjust to these varying complexities distinguishes it from other methods. Without the DGCFE and MRDG components, model performance drops significantly, as evidenced by the elevated CD values of 6.04 cm and 6.21 cm during the flowering and silique stages,

respectively. This performance degradation emphasizes the importance of these modules in ensuring robust canopy reconstruction across all growth stages. However, despite the inclusion of DGCFF and MRDG, the model’s performance diminishes as the canopy architecture becomes more complex and internal occlusions intensify. This results in a gradual decline in point cloud completion accuracy, suggesting that the current model’s learning capability is not infinite. The model still struggles to extract relevant feature representations, particularly in regions with severe occlusions, where the canopy’s density and overlap of leaves pose additional challenges. These results highlight RP-PCN’s modular design, which effectively combines local feature extraction and multi-resolution strategies to address the challenges posed by complex plant canopy structures. Nonetheless, further refinements in occlusion handling and feature extraction in densely occluded regions will be crucial for improving the model’s generalization and accuracy, especially under real-world conditions with significant canopy overlap.

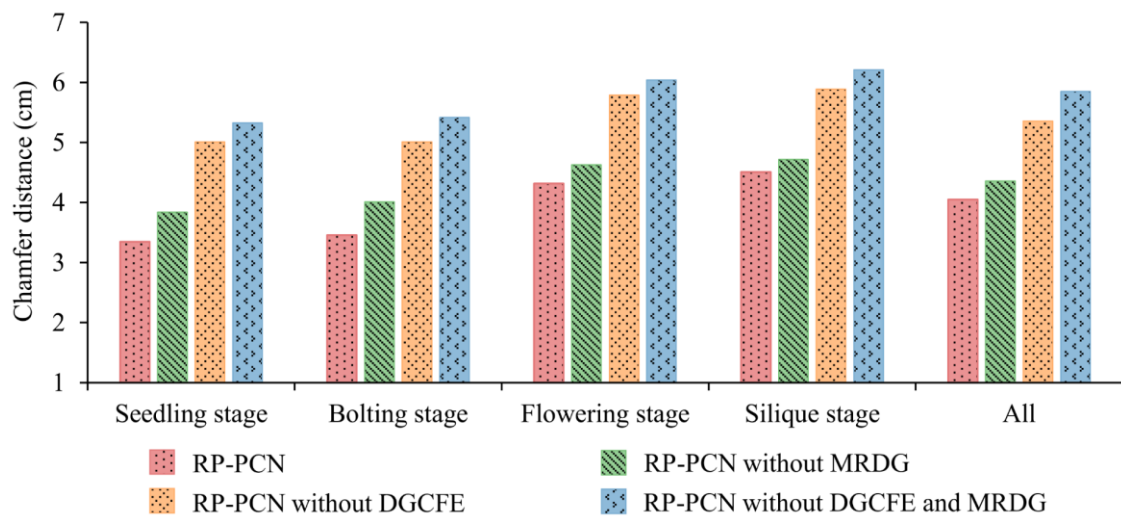


Fig. 12. Results of the ablation study on rapeseed population point cloud completion network (RP-PCN) with different architectures, trained with datasets from seedling,

bolting, flowering, and silique stages, as well as all stages. The chart compares the performance of the full RP-PCN model with versions excluding the dynamic graph convolutional feature extractor (DGCFE) and the multi-resolution dynamic graph (MRDG) individually, as well as a version excluding both components.

In addition to the ablation study, a sensitivity analysis of key hyper-parameters, including the number of nearest neighbors (k), the number of encoder layers (O), and the input and output point cloud sizes (N and M), provided valuable insights into RP-PCN's performance (Fig. 13). The k was found to stabilize the model's performance when set above 20, indicating that this value was optimal for capturing spatial relationships without unnecessary computational overhead. Similarly, the O was most effective at five layers, providing an ideal balance between depth and computational efficiency. Fewer layers limited the model's ability to extract high-level features, while deeper layers led to excessive complexity without additional accuracy. Furthermore, the analysis revealed that increasing the N and M beyond 8192 did not result in significant improvements in model accuracy. Larger point clouds only increased point density, which did not enhance the model's ability to capture structural details. These insights suggest that RP-PCN operates efficiently with moderate point cloud sizes, confirming that optimal hyper-parameter selection contributes to both model accuracy and computational efficiency.

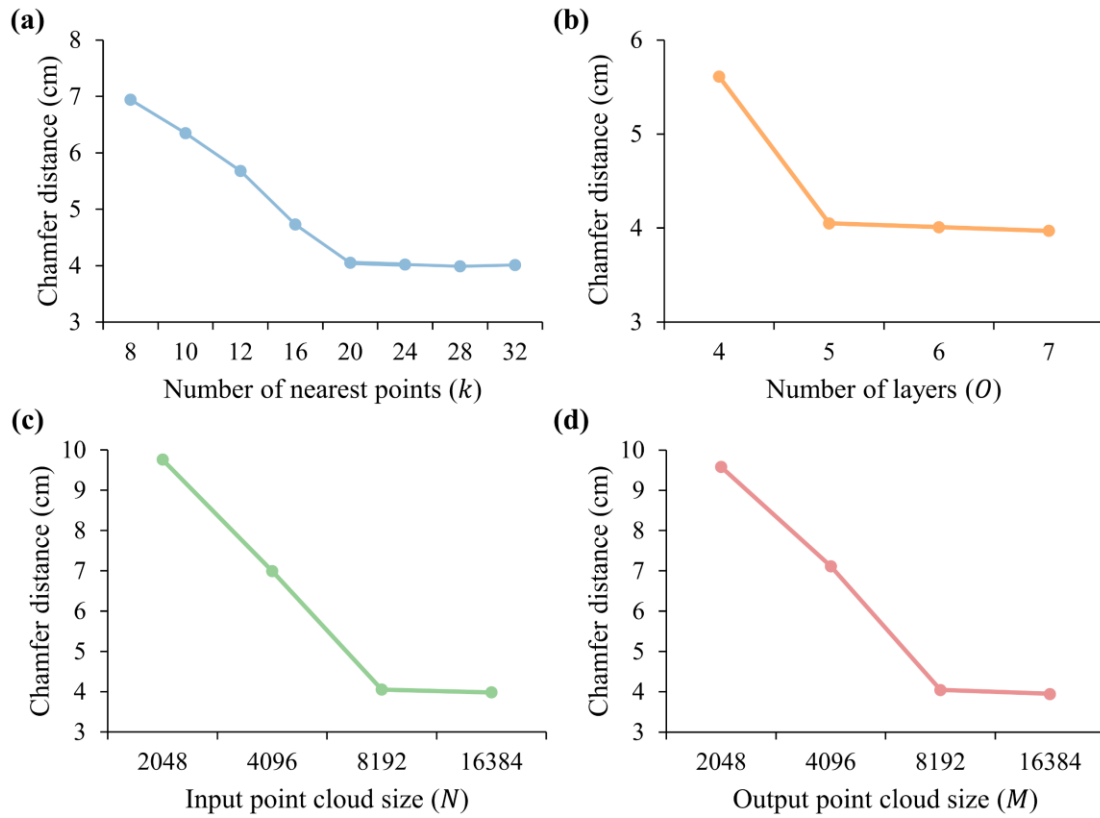


Fig. 13. Sensitivity analysis of (a) the number of nearest neighbors (k), (b) number of layers in the encoder (O), (c) input point cloud size (N), and (d) output point cloud size (M) on the model performance.

5.3 Contribution of RP-PCN on rapeseed population canopy analysis

The RP-PCN model proposed in this study introduces a novel and highly effective approach for obtaining complete architectural information of plant population canopies. Experimental validation with rapeseed canopies demonstrated that point clouds completed by RP-PCN significantly outperformed incomplete point clouds in terms of yield estimation accuracy. Traditionally, rapeseed yield has been estimated using silique-related traits, such as number, length, and weight, which are typically measured without considering the spatial distribution of siliques within the canopy (Zheng et al., 2022). However, the spatial heterogeneity of the canopy and the unique plant

architecture of rapeseed at different growth stages make this estimation challenging. The complete point cloud of rapeseed population by using RP-PCN enables a more accurate representation of the rapeseed canopy. In our study, we divided the canopy of rapeseed into three vertical layers, including upper, middle, and lower layers, to evaluate the yield contribution of each layer. The results showed that siliques in the middle layer had the strongest correlation with overall yield, indicated by their higher silique volume and more efficient light capture compared to the upper and lower layers. Quantification of canopy architectures would help on machine-based description of canopy formation and development, which would open new doors of agronomic trait collection and yield estimation criteria. The parameters extracted by RP-PCN would be used as new agronomic digital traits and further co-analyzed with genomic information for the identification of novel genetic loci. By using digital traits as the input, high-throughput and time-series identification of genetic trait transition switches could be likely uncovered, which would shed light on creative ways of genetic improvement for ideal canopy structures under different circumstances.

The code and dataset preparation methods used for model training in this study have been fully made available for public access. To apply the RP-PCN model to other crops, users only need to follow the procedures outlined in this research to recreate the necessary dataset and train the model accordingly. The time required for this step varies based on the sample size and available hardware resources, and can span a wide range. As a reference, Appendix A.2 provides the time required for dataset preparation and model training under the hardware conditions used in this study. Once the model is

trained, it can be directly applied to new crops without the need for further adjustments. In terms of model application, the time required to complete a single rapeseed field plot is approximately 350 seconds, with most of this time spent on pose estimation and 3D reconstruction. The actual point cloud completion, however, only takes a few seconds using the RP-PCN. While the overall processing time per plot is several minutes, this duration is acceptable for high-throughput phenotyping applications where real-time processing is not typically a strict requirement. If lidar-based devices were used to directly capture the crop surface point clouds, the need for 3D reconstruction would be eliminated, allowing the raw point clouds to be input directly into the model. This would reduce the time required for point cloud completion to just the inference time, which takes only a few seconds.

6. Conclusions

This study introduces a novel approach for obtaining complete canopy architectures of field-grown rapeseed crop populations across different growth stages. By utilizing complete individual plant data collected under field conditions and combining individuals with diverse morphological traits, the proposed method successfully simulates population architectures, achieving state-of-the-art similarity with real-world scenarios. To address the challenges of dataset creation for deep learning, we developed a novel occlusion point detection algorithm, leveraging canopy completion point clouds and triangular mesh. This innovative approach facilitated the creation of a point cloud completion training dataset that accurately reflects the complexities of real-world conditions. The RP-PCN model, which leverages a GAN

architecture and incorporates the MRDG and DGCFE modules, enables efficient feature extraction across varying scales, resulting in superior performance in the completion of rapeseed population point clouds. Additionally, we proposed the SEI as a novel canopy architecture evaluation metric for estimating yield, with results demonstrating that complete canopy architectures markedly improved the accuracy of rapeseed yield estimation. As algorithms for extracting complex structural features continue to evolve and with the optimization of hardware technologies such as parallel computing, RP-PCN's capability to complete complex canopy structures in later growth stages will be further enhanced, along with its computational efficiency. Given the successful application of RP-PCN to rapeseed, we are confident in its ability to be extended to other crops with complex canopy structures. RP-PCN holds great potential as a high-precision phenotyping tool in precision agriculture, contributing to the development of more resilient and high-yielding crop varieties.

Acknowledgements

This work was supported by the National Natural Science Foundation of China (32371985) and the International S&T Cooperation Program of China (2024YFE0115000). We extend our heartfelt gratitude to Ruisen Wang, Yi Feng, Mengjie Gong and Guangyu Wu, for their participation in the experiments, and to the Jiaxing Academy of Agricultural Sciences for their assistance with the experimental data acquisition.

Availability of supporting data and source code

All source codes and test data involved in this study are available on GitHub (<https://github.com/Ziyue-Guo/RP-PCN.git>).

Declaration of Competing Interest

The authors declare that they have no known competing financial interests or personal relationships that could have appeared to influence the work reported in this paper.

Contributions

Z. G. designed the study, conducted the experiments, and wrote the manuscript. Y. S. contributed to the experimental design and data collection. X. Y. assisted with model development and data analysis. Y. Z. and L. J. provided the experimental materials and contributed to the experimental design. H. C. supervised the study and revised the manuscript.

Appendix

A.1 Visualization of RP-PCN completion results

Fig. A1 presents the point cloud completion results generated by RP-PCN at different growth stages. Through slicing along the X, Y, and Z planes, the internal completion of the crop population canopy is showcased. It is evident that RP-PCN performs well in reconstructing both relatively simple structures during the seedling stage and the more complex architectures during the flowering and silique stages. This highlights the model's robust capability to effectively handle a wide range of canopy complexities.

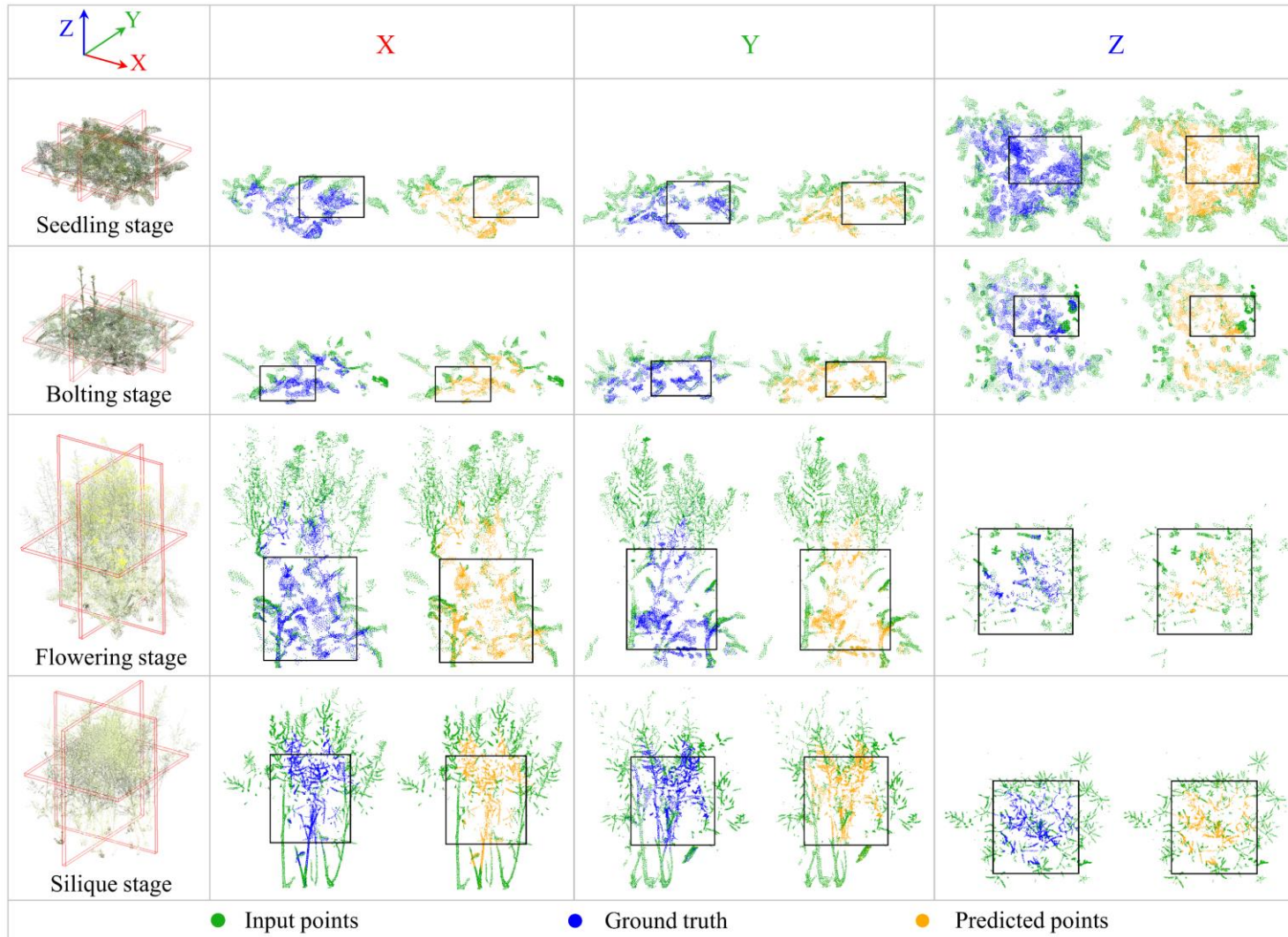


Fig. A1. Visualization of RP-PCN point cloud completion results across different growth stages. The input points (green), ground truth (blue), and predicted points (orange) are shown for each stage: seedling, bolting, flowering, and silique. The black boxes highlight the magnified regions displayed in Fig. 6, where the detailed comparisons between ground truth and predicted points are further illustrated.

A. 2 Processing time for model construction and application

Under the hardware and parameter conditions used in this study (see Section 3.3), re-training the model for a different crop takes approximately 150 hours (Table A2). While this time investment may seem lengthy, it is a one-time process for each crop, making it a reasonable investment for developing a robust, crop-specific model. Once trained, the model can be applied to large-scale phenotyping without requiring further modifications. When applying a pre-trained model for rapeseed point cloud completion, processing a single field plot takes approximately 350 seconds. The majority of this time is spent on pose estimation and 3D reconstruction, while the actual inference of missing point clouds using RP-PCN requires only a few seconds. Despite the overall processing time per plot being several minutes, this duration is acceptable for high-throughput phenotyping applications, as real-time processing is typically not a strict requirement. In practical field experiments, point cloud completion is generally performed as a post-processing step after data collection, which aligns well with real-world agricultural workflows.

Table A2. Processing time for model construction and application phases

| | Step | Time cost |
|-----------------------|--|--------------------------|
| Model Construction | Pose estimation | 300 seconds / 150 images |
| | NeRF training | 180 seconds |
| | Building point cloud completion data set | 120 seconds / plot |
| | Training point cloud completion model | 15 hours |
| | Pose estimation | 100 seconds / 36 images |

| | | |
|-------------|-----------------|-------------|
| Model | NeRF training | 180 seconds |
| Application | Model inference | 2 seconds |

References

- Alexiou, E., Ebrahimi, T., 2020. Towards a Point Cloud Structural Similarity Metric, in: 2020 IEEE International Conference on Multimedia & Expo Workshops (ICMEW). Presented at the 2020 IEEE International Conference on Multimedia & Expo Workshops (ICMEW), pp. 1–6. <https://doi.org/10.1109/ICMEW46912.2020.9106005>
- Arshad, M.A., Jubery, T., Afful, J., Jignasu, A., Balu, A., Ganapathysubramanian, B., Sarkar, S., Krishnamurthy, A., 2024. Evaluating Neural Radiance Fields for 3D Plant Geometry Reconstruction in Field Conditions. *Plant Phenomics* 6, 0235. <https://doi.org/10.34133/plantphenomics.0235>
- Bailey, B.N., Mahaffee, W.F., 2017. Rapid measurement of the three-dimensional distribution of leaf orientation and the leaf angle probability density function using terrestrial LiDAR scanning. *Remote Sensing of Environment* 194, 63–76. <https://doi.org/10.1016/j.rse.2017.03.011>
- Charles, R.Q., Su, H., Kaichun, M., Guibas, L.J., 2017. PointNet: Deep Learning on Point Sets for 3D Classification and Segmentation, in: 2017 IEEE Conference on Computer Vision and Pattern Recognition (CVPR). Presented at the 2017 IEEE Conference on Computer Vision and Pattern Recognition (CVPR), IEEE, Honolulu, HI, pp. 77–85. <https://doi.org/10.1109/CVPR.2017.16>
- Chen, H., Liu, S., Wang, Congyue, Wang, Chaofeng, Gong, K., Li, Y., Lan, Y., 2023. Point Cloud Completion of Plant Leaves under Occlusion Conditions Based on Deep Learning. *Plant Phenomics* 5, 0117. <https://doi.org/10.34133/plantphenomics.0117>
- Du, R., Ma, Z., Xie, P., He, Y., Cen, H., 2023. PST: Plant segmentation transformer for 3D point clouds of rapeseed plants at the podding stage. *ISPRS Journal of Photogrammetry and Remote Sensing* 195, 380–392. <https://doi.org/10.1016/j.isprsjprs.2022.11.022>
- Fei, B., Yang, W., Chen, W.-M., Li, Z., Li, Y., Ma, T., Hu, X., Ma, L., 2022. Comprehensive Review of Deep Learning-Based 3D Point Cloud Completion Processing and Analysis. *IEEE Transactions on Intelligent Transportation Systems* 23, 22862–22883. <https://doi.org/10.1109/TITS.2022.3195555>
- Ge, Y., Xiong, Y., From, P.J., 2020. Symmetry-based 3D shape completion for fruit localisation for harvesting robots. *Biosystems Engineering* 197, 188–202. <https://doi.org/10.1016/j.biosystemseng.2020.07.003>
- Geiger, A., Lenz, P., Stiller, C., Urtasun, R., 2013. Vision meets robotics: The KITTI dataset. *The International Journal of Robotics Research* 32, 1231–1237. <https://doi.org/10.1177/0278364913491297>
- He, K., Zhang, X., Ren, S., Sun, J., 2016. Deep Residual Learning for Image Recognition. Presented

- at the Proceedings of the IEEE Conference on Computer Vision and Pattern Recognition, pp. 770–778.
- Huang, Z., Yu, Y., Xu, J., Ni, F., Le, X., 2020. PF-Net: Point Fractal Network for 3D Point Cloud Completion, in: 2020 IEEE/CVF Conference on Computer Vision and Pattern Recognition (CVPR). Presented at the 2020 IEEE/CVF Conference on Computer Vision and Pattern Recognition (CVPR), IEEE, Seattle, WA, USA, pp. 7659–7667. <https://doi.org/10.1109/CVPR42600.2020.00768>
- Jiang, S., Jiang, C., Jiang, W., 2020. Efficient structure from motion for large-scale UAV images: A review and a comparison of SfM tools. *ISPRS Journal of Photogrammetry and Remote Sensing* 167, 230–251. <https://doi.org/10.1016/j.isprsjprs.2020.04.016>
- Jin, S., Sun, X., Wu, F., Su, Y., Li, Y., Song, S., Xu, K., Ma, Q., Baret, F., Jiang, D., Ding, Y., Guo, Q., 2021. Lidar sheds new light on plant phenomics for plant breeding and management: Recent advances and future prospects. *ISPRS Journal of Photogrammetry and Remote Sensing* 171, 202–223. <https://doi.org/10.1016/j.isprsjprs.2020.11.006>
- Li, M., Shamshiri, R.R., Schirrmann, M., Weltzien, C., Shafian, S., Laursen, M.S., 2022. UAV Oblique Imagery with an Adaptive Micro-Terrain Model for Estimation of Leaf Area Index and Height of Maize Canopy from 3D Point Clouds. *Remote Sensing* 14, 585. <https://doi.org/10.3390/rs14030585>
- Li, N., Li, J., Tung, S.A., Shi, X., Hao, X., Shi, F., Wahid, M.A., Ali, B., Rashid, R., Wang, J., Luo, H., 2022. Optimal irrigation amount can increase cotton lint yield by improving canopy structure and microenvironment under non-film deep drip irrigation. *Journal of Cleaner Production* 360, 132156. <https://doi.org/10.1016/j.jclepro.2022.132156>
- Lin, G., Li, H., Yang, Z., Ruan, Y., Liu, C., 2024. Pod canopy staggered-layer cultivation increases rapeseed (*Brassica napus* L.) yield by improving population canopy structure and fully utilizing light-energy resources. *European Journal of Agronomy* 158, 127229. <https://doi.org/10.1016/j.eja.2024.127229>
- Liu, F., Song, Q., Zhao, J., Mao, L., Bu, H., Hu, Y., Zhu, X.-G., 2021. Canopy occupation volume as an indicator of canopy photosynthetic capacity. *New Phytologist* 232, 941–956. <https://doi.org/10.1111/nph.17611>
- Lou, M., Lu, J., Wang, L., Jiang, H., Zhou, M., 2022. Growth parameter acquisition and geometric point cloud completion of lettuce. *Front. Plant Sci.* 13. <https://doi.org/10.3389/fpls.2022.947690>
- Ma, Z., Du, R., Xie, J., Sun, D., Fang, H., Jiang, L., Cen, H., 2023. Phenotyping of Siliques Morphology in Oilseed Rape Using Skeletonization with Hierarchical Segmentation. *Plant Phenomics* 5, 0027. <https://doi.org/10.34133/plantphenomics.0027>
- Magistri, F., Marcuzzi, R., Marks, E., Sodano, M., Behley, J., Stachniss, C., 2024. Efficient and Accurate Transformer-Based 3D Shape Completion and Reconstruction of Fruits for Agricultural Robots, in: 2024 IEEE International Conference on Robotics and Automation (ICRA). Presented at the 2024 IEEE International Conference on Robotics and Automation (ICRA), pp. 8657–8663. <https://doi.org/10.1109/ICRA57147.2024.10611717>
- Masuda, T., 2021. Leaf Area Estimation by Semantic Segmentation of Point Cloud of Tomato Plants. Presented at the Proceedings of the IEEE/CVF International Conference on Computer Vision, pp. 1381–1389.
- Müller, T., Evans, A., Schied, C., Keller, A., 2022. Instant neural graphics primitives with a

- multiresolution hash encoding. *ACM Trans. Graph.* 41, 102:1-102:15. <https://doi.org/10.1145/3528223.3530127>
- Murchie, E.H., Burgess, A.J., 2022. Casting light on the architecture of crop yield. *Crop and Environment* 1, 74–85. <https://doi.org/10.1016/j.crope.2022.03.009>
- Paullada, A., Raji, I.D., Bender, E.M., Denton, E., Hanna, A., 2021. Data and its (dis)contents: A survey of dataset development and use in machine learning research. *PATTER* 2. <https://doi.org/10.1016/j.patter.2021.100336>
- Rossi, R., Costafreda-Aumedes, S., Summerer, S., Moriondo, M., Leolini, L., Cellini, F., Bindi, M., Petrozza, A., 2022. A comparison of high-throughput imaging methods for quantifying plant growth traits and estimating above-ground biomass accumulation. *European Journal of Agronomy* 141, 126634. <https://doi.org/10.1016/j.eja.2022.126634>
- Sun, B., Wang, C., Yang, C., Xu, B., Zhou, G., Li, X., Xie, J., Xu, S., Liu, B., Xie, T., Kuai, J., Zhang, J., 2021. Retrieval of rapeseed leaf area index using the PROSAIL model with canopy coverage derived from UAV images as a correction parameter. *International Journal of Applied Earth Observation and Geoinformation* 102, 102373. <https://doi.org/10.1016/j.jag.2021.102373>
- Tchapmi, L.P., Kosaraju, V., Rezatofighi, H., Reid, I., Savarese, S., 2019. TopNet: Structural Point Cloud Decoder. Presented at the Proceedings of the IEEE/CVF Conference on Computer Vision and Pattern Recognition, pp. 383–392.
- Vaswani, A., Shazeer, N., Parmar, N., Uszkoreit, J., Jones, L., Gomez, A.N., Kaiser, Ł., Polosukhin, I., 2017. Attention is all you need, in: Proceedings of the 31st International Conference on Neural Information Processing Systems, NIPS'17. Curran Associates Inc., Red Hook, NY, USA, pp. 6000–6010.
- Wang, Y., Sun, Y., Liu, Z., Sarma, S.E., Bronstein, M.M., Solomon, J.M., 2019. Dynamic Graph CNN for Learning on Point Clouds. *ACM Trans. Graph.* 38, 1–12. <https://doi.org/10.1145/3326362>
- Watawana, B., Isaksson, M., 2024. Automated microgreen phenotyping for yield estimation using a consumer-grade depth camera. *Smart Agricultural Technology* 7, 100384. <https://doi.org/10.1016/j.atech.2023.100384>
- Wu, T., Pan, L., Zhang, J., WANG, T., Liu, Z., Lin, D., 2021. Balanced Chamfer Distance as a Comprehensive Metric for Point Cloud Completion, in: Advances in Neural Information Processing Systems. Curran Associates, Inc., pp. 29088–29100.
- Wu, Z., Song, S., Khosla, A., Yu, F., Zhang, L., Tang, X., Xiao, J., 2015. 3D ShapeNets: A Deep Representation for Volumetric Shapes. Presented at the Proceedings of the IEEE Conference on Computer Vision and Pattern Recognition, pp. 1912–1920.
- Xie, H., Yao, H., Zhou, S., Mao, J., Zhang, S., Sun, W., 2020. GRNet: Gridding Residual Network for Dense Point Cloud Completion, in: Vedaldi, A., Bischof, H., Brox, T., Frahm, J.-M. (Eds.), *Computer Vision – ECCV 2020*, Lecture Notes in Computer Science. Springer International Publishing, Cham, pp. 365–381. https://doi.org/10.1007/978-3-030-58545-7_21
- Yu, X., Rao, Y., Wang, Z., Liu, Z., Lu, J., Zhou, J., 2021. PoinTr: Diverse Point Cloud Completion with Geometry-Aware Transformers, in: 2021 IEEE/CVF International Conference on Computer Vision (ICCV). Presented at the 2021 IEEE/CVF International Conference on Computer Vision (ICCV), IEEE, Montreal, QC, Canada, pp. 12478–12487.

<https://doi.org/10.1109/ICCV48922.2021.01227>

Zhang, Y., Su, W., Tao, W., Li, Z., Huang, X., Zhang, Z., Xiong, C., 2023. Completing 3D Point Clouds of Thin Corn Leaves for Phenotyping Using 3D Gridding Convolutional Neural Networks. *Remote Sensing* 15, 5289. <https://doi.org/10.3390/rs15225289>

Zheng, M., Terzaghi, W., Wang, H., Hua, W., 2022. Integrated strategies for increasing rapeseed yield. *Trends in Plant Science, Special issue: Climate change and sustainability II* 27, 742–745. <https://doi.org/10.1016/j.tplants.2022.03.008>